Journal of Luminescence 171 (2016) 33–39

Contents lists available at ScienceDirect

Journal of Luminescence

journal homepage: www.elsevier.com/locate/jlumin

Full Length Article

Bandgap engineering of the $Lu_xY_{1-x}PO_4$ mixed crystals

V.S. Levushkina [a,b,*], D.A. Spassky [a,c], E.M. Aleksanyan [a,d], M.G. Brik [a,e,f,g], M.S. Tretyakova [h], B.I. Zadneprovski [h], A.N. Belsky [i]

[a] Institute of Physics, University of Tartu, Ravila 14c, 50411 Tartu, Estonia
[b] Physics Faculty, Moscow State University, Leninskiye Gory 1-2, 11991 Moscow, Russia
[c] Skobeltsyn Institute of Nuclear Physics, Moscow State University, Leninskiye Gory 1-2, 11991 Moscow, Russia
[d] A. Alikhanyan National Science Laboratory, Yerevan Physics Institute, Alikhanyan Yeghbayrneri St. 2, 0036 Yerevan, Armenia
[e] College of Sciences, Chongqing University of Posts and Telecommunications, 400065 Chongqing, PR China
[f] Institute of Physics, Jan Dlugosz University, Armii Krajowej 13/15, PL-42200 Czestochowa, Poland
[g] Institute of Physics, Polish Academy of Sciences, Al. Lotników 32/46, 02-668 Warsaw, Poland
[h] Central Research and Development Institute of Chemistry and Mechanics, Nagatinskaya St. 16a, 115487 Moscow, Russia
[i] Institute of Light and Matter, CNRS, University Lyon1, 69622 Villeurbanne, France

ARTICLE INFO

Article history:
Received 16 May 2015
Received in revised form
21 October 2015
Accepted 30 October 2015
Available online 10 November 2015

Keywords:
Mixed crystals
$LuPO_4$
YPO_4
Thermostimulated luminescence
Ab-initio calculation
Bandgap engineering

ABSTRACT

Bandgap modification of the $Lu_xY_{1-x}PO_4$ mixed crystals has been studied by thermostimulated luminescence (TSL) and ab-initio calculation methods. Doping of $Lu_xY_{1-x}PO_4$ with Ce^{3+} allowed to follow up the changes of electron traps depth, caused by the modification of the bottom of conduction band. The observed gradual shift of the most intensive TSL peaks to higher temperatures with increase of x value was connected with the high-energy shift of the conduction band bottom. According to the band structure calculations the bottom of the conduction band is formed by the 5d and 4d states of Lu and Y, respectively. Therefore, substitution of one cation by another is responsible for the observed variation of the electronic and optical properties. Doping with Eu^{3+} was used to study the modification of the hole traps and the top of the valence band in $Lu_xY_{1-x}PO_4$. The independence of the TSL peaks position on x value in $Lu_xY_{1-x}PO_4$:Eu^{3+} allows to conclude that the top of the valence band is negligibly affected by the cation substitution. According to the band structure calculations the top of the valence band is formed by the O 2p electronic states, which are not affected by the cation substitution. The resulting increase of the bandgap with x value is confirmed by the data of ab-initio calculations.

1. Introduction

Phosphates with chemical formula APO_4:RE (A=Y or Lu and RE stands for any rare earth element) are promising materials with excellent luminescent properties, high chemical and thermal stability and radiation resistance [1–8]. Such phosphates are used in various applications: scintillation detectors, phosphors for X-ray imaging and plasma display panels as well as the host materials for radioactive waste storage [2,9–14].

Recently, a special attention was focused on studies of the mixed crystals, whose scintillation properties in some cases surpass those of the pure crystals without any intentional additions. A non-linear effect of the increase of the efficiency of excitation energy conversion into luminescence, which leads to an increase of the scintillation light yield, has been reported in Refs. [15–21]. Moreover, engineering of the band gap of mixed crystals allows for tuning properties of such compounds, e.g. to reduce the adverse influence of point defects on the scintillation properties [22]. The point defects usually occur in oxides (like oxygen vacancies, for example); they manifest themselves by the discrete energy levels in the host's bandgap, which can trap free charge carriers. This results either in (i) suppression of the light output when charge carriers cannot be thermally released from the traps or in (ii) delayed recombination when the thermal release of those trapped carriers is possible. Development of the mixed crystals allows to prevent the free carrier's trapping, even in the case when defect's concentration is not reduced. For instance, doping of $Lu_3Al_5O_{12}$ by Ga^{3+} ions results in the decrease of the bandgap energy; the defect states – due to the band gap narrowing after doping – become buried under the conduction band states [22].

In this work we have studied modification of the band structure of the $Lu_xY_{1-x}PO_4$ mixed crystals with the gradual substitution of Y by Lu in the whole range of concentration x from 0 to 1. Bandgap changes caused by variation of the chemical composition were followed by studies of the thermostimulated luminescence

* Corresponding author. Institute of Physics, University of Tartu, Ravila 14c, 50411 Tartu, Estonia.
E-mail address: viktoriia.levushkina@ut.ee (V.S. Levushkina).

http://dx.doi.org/10.1016/j.jlumin.2015.10.074
0022-2313/

(TSL), which was shown to be an effective method to extract information about carriers' traps existing in phosphates [23–26]. In order to obtain the information about the modification of the bottom of conduction band (CB) and the top of the valence band (VB), the TSL of the samples doped with Ce^{3+} and Eu^{3+} was studied. These experiments were supported by the ab initio calculations of the structural and electronic properties of the studied compounds, in order to shed more light on the composition-driven changes of the electronic band structure.

2. Details of experimental methods and theoretical calculations

Mixed $Lu_xY_{1-x}PO_4$ crystals with different stoichiometry ratio (x=0, 0.1, 0.3, 0.5, 0.7, 0.9, 1.0) doped with 0.5 mol % Ce^{3+} or 0.5 mol % Eu^{3+} were synthesized by the sol–gel method. According to the granulometric analysis, predominant size of the obtained crystalline particles was 350–600 nm. Particles of such dimensions are very attractive for application. From one hand the size of particles exceeds the path length of gamma photons with energy of tens of keV and it allow to consider them as X-ray phosphors [27]. From other hand the size is small enough for the synthesis of transparent ceramics.

The X-ray diffraction patterns (λ=1.5405 Å) of all obtained samples were recorded by a Rigaku Ultima IV X-ray diffractometer. Measurements of the TSL curves were carried out on two experimental set-ups with an X-ray tube and an electron gun as the irradiation sources. X-ray irradiation was performed using an X-ray tube (W-anode, 30 mA and 35 kV) run by an INEL XRG 3000 generator. The TSL curves and luminescence spectra in the TSL peaks were detected using an ANDOR 500i spectrometer with ANDOR Newton CCD camera. The samples were mounted into LINKAM THMS600 Stage, which allowed to perform TSL measurements in the temperature range 80–450 K with linear heating rate 0.167 K/s.

The TSL measurements under irradiation with electrons (5 keV, 0.4 μA, spot ≈ 1mm^2) were performed in the temperature range 80–300 K with a linear heating rate 0.167 K/s. All measurements were carried out in a liquid helium vacuum cryostat (5–400 K temperature range, 2*10^{-7} Torr) equipped with LakeShore 331 Temperature Controller. The TSL curves were detected using the UV–vis–NIR (200–1700 nm) monochromator ARC SpectraPro-2300i equipped with Hamamatsu photon counting head H6240.

The calculations of band structure were carried out for the set of the $Lu_xY_{1-x}PO_4$ (x=0, 0.25, 0.5, 0.75, 1) crystals with the help of the CASTEP module [28] of Materials Studio. The generalized gradient approximation (GGA) with the Perdew–Burke–Ernzerhof [29] was used to treat the exchange-correlation effects. The plane-wave basis set cut off energy was set at 380 eV; the Monkhorst–Pack k-points mesh was 2 × 2 × 2 for the structural optimization and 4 × 4 × 4 for the calculations of optical properties; the electronic configurations were the following: $4d^15s^2$ for Y, $4f^{14}5p^65d^16s^2$ for Lu, $3s^23p^3$ for P and $2s^22p^4$ for O.

3. Results and discussion

3.1. Ab-initio calculations

At ambient conditions, both YPO_4 and $LuPO_4$ have the same structure described by the tetragonal space group I41/amdZ with the lattice constants (in Å): a=6.8817; c=6.0177 (YPO_4) and a=6.7920, c=5.9540 ($LuPO_4$) [30] with four formula units per one unit cell. At first, one unit cell was optimized for pure YPO_4. Then four atoms of Y were replaced one by one by atoms of Lu, to model

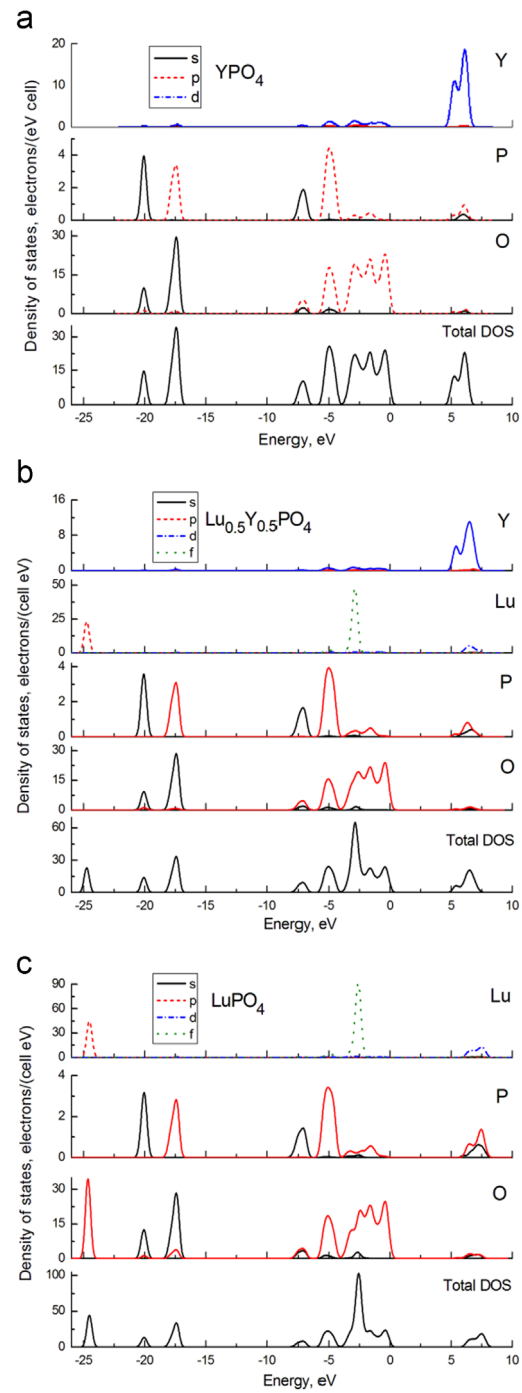

Fig. 1. Calculated density of states diagrams for YPO_4 (a), $Lu_{0.5}Y_{0.5}PO_4$ (b), $LuPO_4$ (c) (x=0, 0.5, 1) compounds.

the following compositions: $Lu_{0.25}Y_{0.75}PO_4$, $Lu_{0.5}Y_{0.5}PO_4$, $Lu_{0.75}Y_{0.25}PO_4$ and $LuPO_4$.

The calculated DOS of some of the studied mixed crystals are shown in Fig. 1. The CB is made of the 4d/5d states of Y/Lu, with a small contribution of the 2p/3p states of O/P, which arise due to the hybridization effects after the chemical bonds between the anions and cations are formed. The structure of the VB exhibits several sub-bands. The upper one between −4 and 0 eV is due to the 2p states of O, whereas two lower sub-bands peaked at about −7 and −5 eV arise from the 3s, 3p states of P. The completely filled 4f shell of Lu produces a sharp maximum at about −2.5 eV in the valence band. Deeper bands localized at −25 eV, −20 eV

and −17.5 eV are due to the Lu 5p states, O 2s states, O and P 2s,2p/3s, 3p states, respectively.

The calculated dependence of the band gap on the value x in the $Lu_xY_{1-x}PO_4$ series of compounds is presented in Fig. 2. It demonstrates a linear increase of the band gap value with the increase of the concentration of Lu in $Lu_xY_{1-x}PO_4$. It is worth noting that the calculated values of the bandgap are lower than the experimental values of 8.8–9.2 eV available from the literature [31–33]. The underestimation of the calculated band gap is a common feature of the DFT-based calculations and is explained by not taking into account the discontinuity in the exchange-correlation potential [34].

3.2. X-ray powder diffraction analysis of $Lu_xY_{1-x}PO_4$

The X-ray powder diffraction (XRD) patterns of $Lu_xY_{1-x}PO_4$:Ce^{3+} powders are presented in Fig. 3. As follows from the XRD patterns, the synthesized phosphates are homogeneous and well-structured compounds with tetragonal space group I41/amdZ, and consistent with the data of ICSD#162336 ($LuPO_4$) and ICSD#184543 ($LuPO_4$). Doping of $Lu_xY_{1-x}PO_4$ mixed crystals with Eu^{3+} does not change the XRD pattern. The shift of the diffraction

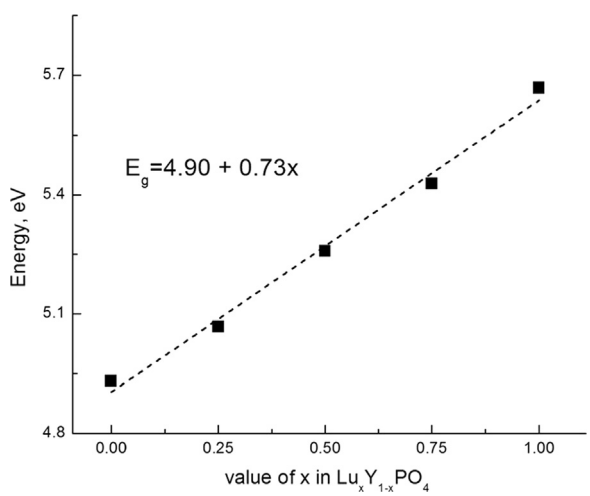

Fig. 2. The calculated band gap of $Lu_xY_{1-x}PO_4$ mixed crystals.

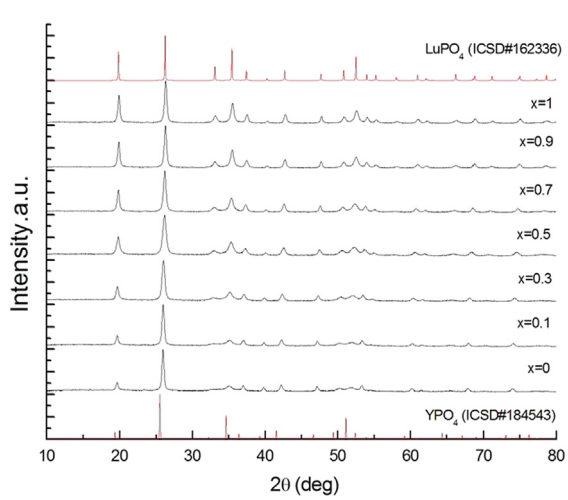

Fig. 3. XRD patterns of $Lu_xY_{1-x}PO_4$:Ce^{3+}. The red line spectrum represents literature data for $LuPO_4$ according to ICSD#162336 and YPO_4 according to ICSD#184543. (For interpretation of the references to color in this figure legend, the reader is referred to the web version of this article.)

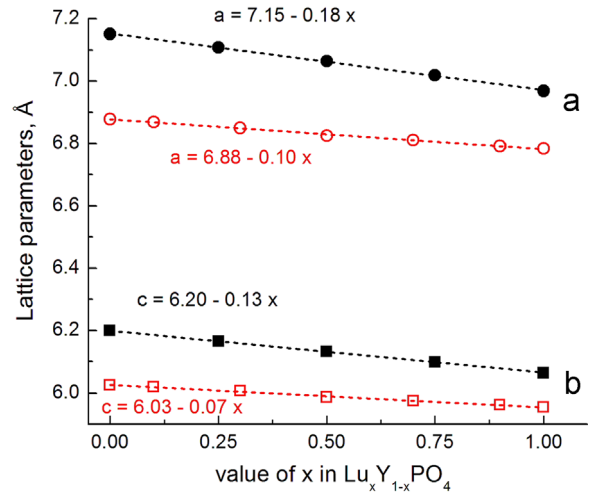

Fig. 4. Experimental (empty circles) and calculated (filled circles) values of lattice parameters a and c of $Lu_xY_{1-x}PO_4$ mixed crystals.

lines to greater 2θ value with increase of the x value was detected. Such behavior of the diffraction lines is connected with change of the lattice parameters in the set of the studied mixed crystals. According to the XRD pattern the experimental parameters of the unit cell increase from $LuPO_4$ to YPO_4 that is in a good agreement with the results of calculations. The dependence of the calculated and experimental lattice constants a and c of the mixed crystals on the x value is presented in Fig. 4. The calculated data were optimized with the relative error of about 4% for the a constant and 2% for the c constant for pure compounds. The dependencies of experimental as well as calculated constant's values on x follow the Vegards's law and can be fitted to the linear functions, which are also given in Fig. 4. The differences between experimental and calculated lattice parameters are always present, that is associated with the optimized structure, which always corresponds to the lowest energy of the crystal lattice.

3.3. Thermally stimulated luminescence of $Lu_xY_{1-x}PO_4$:Ce^{3+}

The TSL curves of Ce^{3+} doped mixed crystals are shown in Fig. 5. The curves consist of two groups of peaks in the ranges between 85–125 K and 130–275 K. The TSL curve of the YPO_4:Ce^{3+} consists of a peak with maximum at 110 K (peak A), and two overlapping peaks at 160 K (peak B) and 180 K (peak C). With increase of the x value the structure of the TSL curves changes in the following way. The presence of two overlapping peaks (denoted as A and A′) with maxima at 100 K and 120 K can be observed for the samples with $x=0.1$, 0.7, 0.9. A single broad peak A was detected again in the samples with $x=0.3$, 0.5, while in case of $x=1$ none of these peaks was not observed.

The profile of the complex TSL peak in the range 130–275 K changes as well. The most prominent tendency is the gradual shift of this group of peaks to higher temperature with increase of the x value. In addition, starting from $x=0.3$ the peak B cannot be observed separately because of the decrease of its intensity and strong overlap with peak C. Actually the broadening of peak C was observed for the samples with $x=0.3$ and $x=0.5$. In case of $x>0.5$, on the contrary, narrowing of this peak was detected.

So far, as the Ce^{3+} ion is a stable hole trap [35], we assume that the observed peaks are connected with the thermal release of electrons from traps in the mixed phosphates. The recombination process, which is responsible for the observed TSL peaks, can be described in the following way. After excitation the holes are trapped at the Ce^{3+} doping ions, according to the scheme: $Ce^{3+}+h->Ce^{4+}$. When the sample is heated, the electrons are

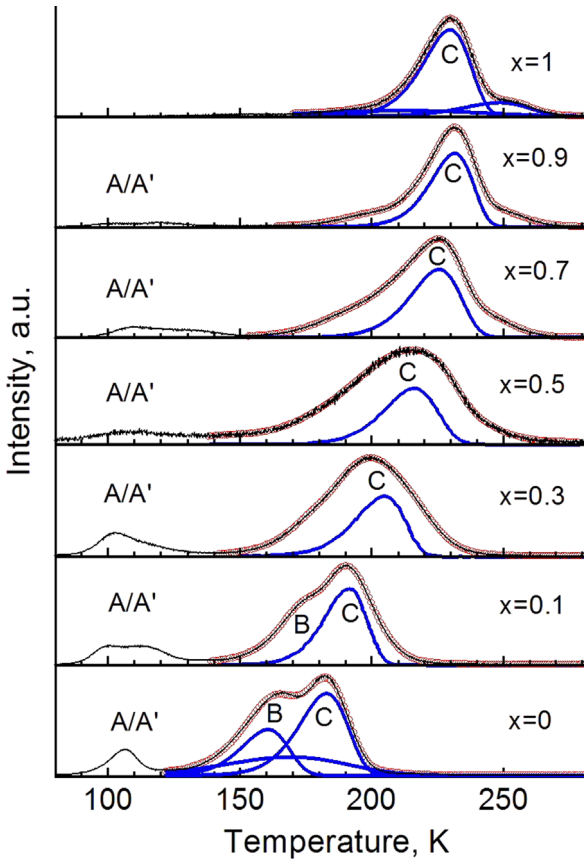

Fig. 5. The TSL curves of $Lu_xY_{1-x}PO_4:Ce^{3+}$ measured after irradiation with X-rays. The fitting of the curves is represented by red hollow circles. Whole set of the elementary peaks used for the fitting is presented for compounds with $x=0$ and 1, while for other compounds only the dominating peak C is presented for a better visualization. (For interpretation of the references to color in this figure legend, the reader is referred to the web version of this article.)

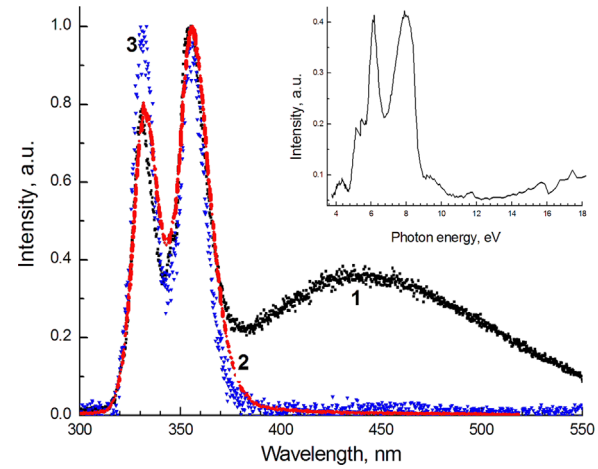

Fig. 6. The steady state luminescence spectrum under X-ray excitation at $T=96$ K (curve 1) and T=300 K (curve2) and luminescence spectrum of the TSL peaks A, B and C (curve 3) of the $YPO_4:Ce^{3+}$. Inset: excitation luminescence spectra of undoped YPO_4, $\lambda_{em}=480$ nm, $T=7$ K.

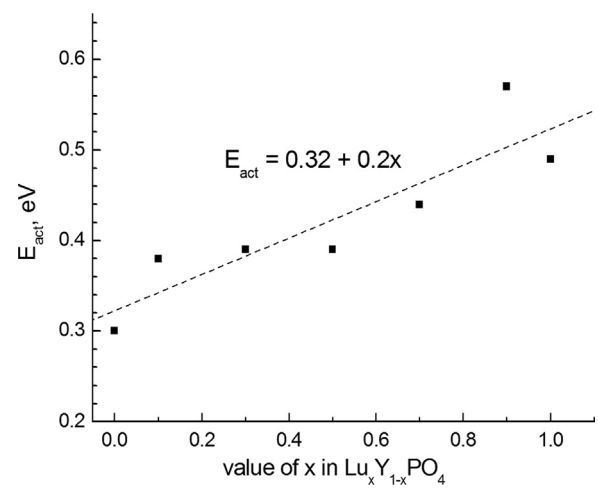

Fig. 7. Dependence of the trap activation energy of the dominant elementary peak on the composition of the $Lu_xY_{1-x}PO_4$ mixed crystals, which was extracted from the TSL curves using the first order kinetics (dots); line fitting of the experimental data (dash line).

thermally released from the traps to the CB and are captured by the Ce^{4+} ions, where they recombine radiatively with the holes left and generate the Ce^{3+} 5d–4f luminescence. In this case the emission spectrum in TSL peaks should consist of the Ce^{3+} emission.

The luminescence spectrum of the TSL peaks is presented in Fig. 6. Two emission bands peaking at 334 nm and 362 nm originated from the 5d–4f transitions on the dopant Ce^{3+} ions were detected. The spectral composition of luminescence in the TSL peaks is similar to the steady state luminescence of crystals in the 320–380 nm range, which is also presented in Fig. 6. Besides the emission band related to Ce^{3+} the additional broad band is observed in the spectral region 380–600 nm in the steady state luminescence spectrum. This band was detected in both, undoped and RE-doped phosphates and is attributed to the defects of crystal structure. The excitation spectrum of this band is presented in the inset of Fig. 6. The emission is excited in transparency region of phosphates while the excitation efficiency rapidly decreases when the excitation energy exceeds the edge of fundamental absorption (~8.8 eV).

The origin of electron traps in the YPO_4 doped with RE was discussed before in Refs. [23–26], where two groups of the TSL peaks were detected as well. The first one consists of two peaks with maxima at around 100 K and 110 K. These peaks were observed only for the crystals doped with Ce^{3+} and are associated with the presence of cerium ions [25,26]. The possibility of electron capture by Ce ions with formation of Ce^{2+} has been discussed in [23,35]. The first exited state 5d of the Ce^{2+} ions is located at 0.38 eV below the bottom of the CB according to [23]. Therefore, the electrons can be captured by Ce ions according to the scheme $Ce^{3+}+e- > 5d^14f^1\ Ce^{2+}$. Based on this assumption, we can suppose that the origin of the A and A′ peaks is associated with the thermal release of electrons from Ce^{2+} and their further recombination with holes on Ce^{4+}.

The second group of TSL peaks is observed in the range from 190 K to 230 K with a maximum at 195 K. This group was fitted by a set of elementary TSL peaks using the first order decay approximation and supposing that the top of VB and bottom of CB are flat. The number of peaks used for approximation varies from 3 to 6 depending on x value. It is minimal for lutetium and yttrium phosphates and maximal for their solid solution with intermediate values of $x=0.5$. This is presumably connected with a partial disorder of the mixed crystals, which results in the increase of variety of trap depths. Approximation allowed to single out the dominating elementary TSL peak, which is labeled as C. The dependence of the activation energy E_{act} of this peak on the composition of the mixed crystals is presented in Fig. 7. A gradual increase of the E_{act} up to ~0.2 eV is observed with the increase of x value in $Lu_xY_{1-x}PO_4$.

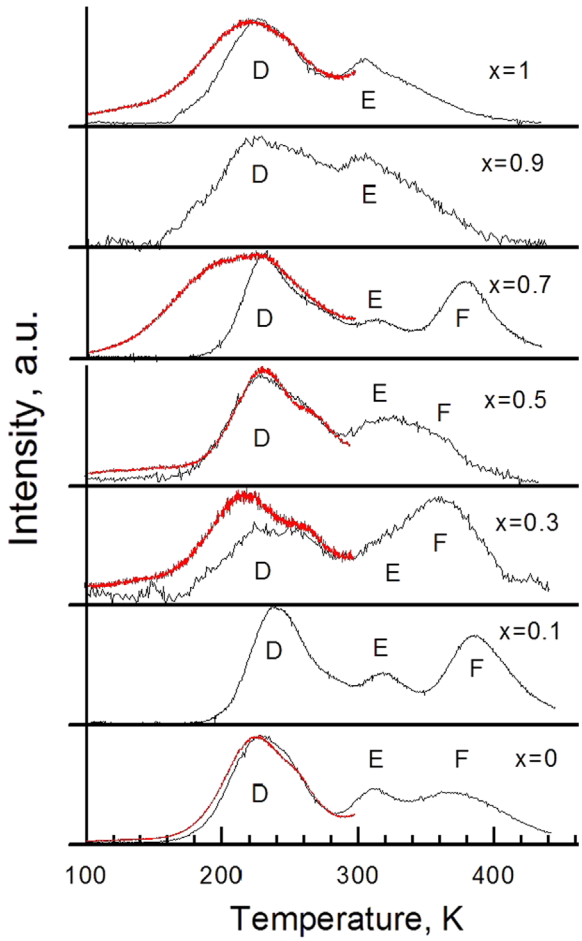

Fig. 8. The TSL curves of $Lu_xY_{1-x}PO_4:Eu^{3+}$ measured after irradiation with X-rays (black curve) and electrons (red curve). (For interpretation of the references to color in this figure legend, the reader is referred to the web version of this article.)

The observed main peak C have been connected with the host defects because these peaks are observed in YPO_4 doped with different RE ions [23]. We suggest that the peak C is associated with host defects, presumably with oxygen vacancies. The trap is not connected with Lu or Y cation sites, because this TSL peak is observed for the whole set of mixed crystals including $LuPO_4$ and YPO_4. For more precise identification of the origin of these point defects some additional studies are needed to be carried out, for example, using the electron paramagnetic resonance (EPR) technique, or by compiling information about the study of other similar phosphates doped with other RE ions.

3.4. Thermally stimulated luminescence of $Lu_xY_{1-x}PO_4:Eu^{3+}$

The TSL curves of mixed crystals doped with Eu^{3+} are shown in Fig. 8. The profiles of curves measured after X-ray and electron irradiation of samples are similar in most cases. Only in the mixed phosphate with $x=0.7$ additional low temperature peak arises after electron irradiation. Further discussion will be related to the data measured after X-ray irradiation of samples because of wider temperature range of measurements. The curves are characterized by several peaks in the temperature region 150–500 K. The TSL curve of the $YPO_4:Eu^{3+}$ consists of a separated peak with a maximum at 225 K (peak D) and two overlapping peaks with maxima at around 310 K (peak E) and 375 K (peak F), accordingly. The position of the peak D fluctuates around 225 K and does not shift when x value changes from 0 to 1. The dependence of the position and relative intensity of the overlapping peaks E and F is more

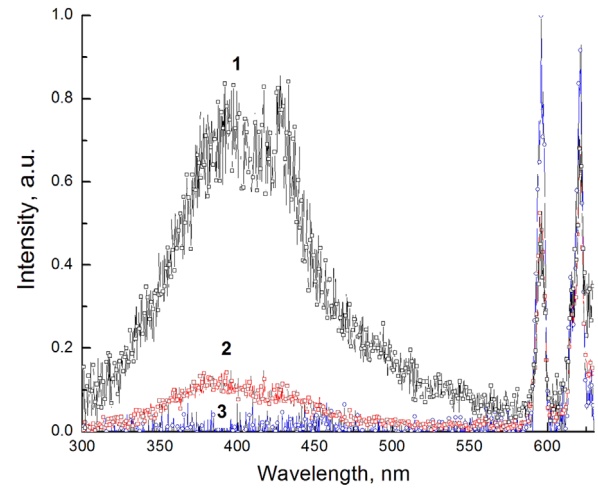

Fig. 9. The steady state luminescence spectra under X-ray excitation at $T=96$ K (curve 1) and $T=300$ K (curve 2) and luminescence spectrum of the TSL peaks D, E and F (curve 3) of $Lu_{0.3}Y_{0.7}PO_4:Eu^{3+}$.

complicated, however it does not follow any clear tendency. We assume that this is connected with a redistribution of an intensity of peaks E and F, which is sample dependent.

Therefore in the case of mixed phosphates doped with Eu^{3+}, positions of the TSL peaks are independent of the value of x. The spectral composition of the steady state luminescence under X-ray excitation and of the luminescence in TSL peaks is presented in Fig. 9. Narrow peaks, which are observed in the 580–640 nm region are ascribed to the Eu^{3+} f–f transitions, and the broad band in the region 300–500 nm is associated with the defect emission as in the case of Ce^{3+} doped phosphates. The luminescence spectra in TSL peaks D, E and F are similar and consist of the emission bands related to the f–f transitions of the Eu^{3+} ion only. The recombination process responsible for the TSL peaks can be described in the following way. After high-energy excitation, the electrons from the CB are trapped at Eu^{3+} doping ions, according to the scheme: $Eu^{3+}+e- > Eu^{2+}$. By thermal activation, the holes from traps are transferred via VB to Eu^{2+}, where they recombine radioactively with the electrons and generate the Eu^{3+} f–f luminescence. Therefore, considering the Eu^{3+} as a stable electron trap, we assume that the observed TSL peaks in the $Lu_xY_{1-x}PO_4:Eu^{3+}$ are connected with the thermal release from the hole traps.

The origin of the hole traps in YPO_4 and $LuPO_4$ is poorly studied. To the best of our knowledge, the origin of the hole traps in the $YPO_4:Eu^{3+}$ and $LuPO_4:Eu^{3+}$ crystals has not been studied before. The TSL measurements for the $YPO_4:Eu^{3+}$, Ce^{3+} were carried out in [36]. The broad non-elementary TSL peak has been observed in the region 320–520 K with a maximum at around 400 K, i.e. in the temperature region, where the peaks E and F are observed. The luminescence spectrum in this peak consists of Eu^{3+} emission and emission of some defect, i.e. it is similar to our results. Therefore, the TSL peak in the 300–450 K range has been observed for the different samples and can be ascribed to the host defects of phosphates.

3.5. Bandgap engineering in $Lu_xY_{1-x}PO_4$

Variation of the chemical composition by substituting one chemical element by another one allows to modify the band structure and to eliminate the adverse influence from defect states on energy transfer process [22]. The shift of the states of CB and VB in the vicinity of the bandgap caused by the substitution of one ion by another one in a mixed crystal may lead to the decrease of the depth of traps, which are associated with defects. In some cases

the states of energy bands envelope the traps and eliminate their influence on the energy transfer processes. We have analyzed the modification of the band gap of $Lu_xY_{1-x}PO_4$ using the results of the TSL measurements and ab initio calculations of the band structure. The presented TSL curves provide with information about a modification of the energy bands in the region of bandgap. The high temperature shift of the TSL peaks B and C in Ce^{3+} doped mixed phosphates indicates the increase of the depth of electron traps with the increase of x value. According to Fig. 7 the change of the E_{act} is up to 0.2 eV. The change of electron trap depth is connected with the shift of the bottom of conduction band relatively to the position of electron traps. It is worth noting that according to [4,35] the bandgap of $LuPO_4$ is larger than that of YPO_4 on 0.2–0.3 eV. Therefore the value of bandgap shift generally corresponds to the change of E_{act}. Thus we suppose that for $Lu_xY_{1-x}PO_4$ the bottom of conduction band shifts to higher energies from YPO_4 to $LuPO_4$ while the position of electron traps is not significantly affected by the cations replacement.

The modification of the CB is also confirmed by the band structure calculations of $Lu_xY_{1-x}PO_4$ (Fig. 1). The bottom of the CB is formed by the 4d/5d mixed states of Y/Lu. The 5d Lu and 4d Y states form – the lower sub-band in CB of the $LuPO_4$ and YPO_4 respectively, but in case of the YPO_4 the CB bottom moves to ~0.73 eV below that one of the $LuPO_4$. It is worth noting that this value exceeds the experimental one. Difference between the calculated and experimentally observed slopes of the band gap variation vs composition can be related to the well-known limitations of the GGA, which considerably underestimates true value of the band gap. These effects of band gap underestimation are especially noticeable when the full cation substitution is accompanied by a relatively small increase of the band gap-about 0.2–0.3 eV in our case, which constitutes only about 2–3% from the band gaps of pure hosts $LuPO_4$ and YPO_4.

In the case of $Lu_xY_{1-x}PO_4$:Eu^{3+}, the position of all TSL peaks does not depend on the x value and the peaks are not shifted. We presume that the position of the top of VB is not changed. According to the band structure calculations, the top of the VB is formed by the 2p states of O with a minor contribution of the 3p and 3s states of P in its lower part and without contribution from Y or Lu states in all studied mixed crystals. Therefore, the substitution of Lu cation by Y one does not affect the top of VB.

In order to confirm the conclusion that the position of the VB's top is not affected by cations's replacement the exitation luminescence spectra of Eu^{3+} emission were measured in the energy region of a charge transfer band (CTB), Fig. 10. CTB is caused by the

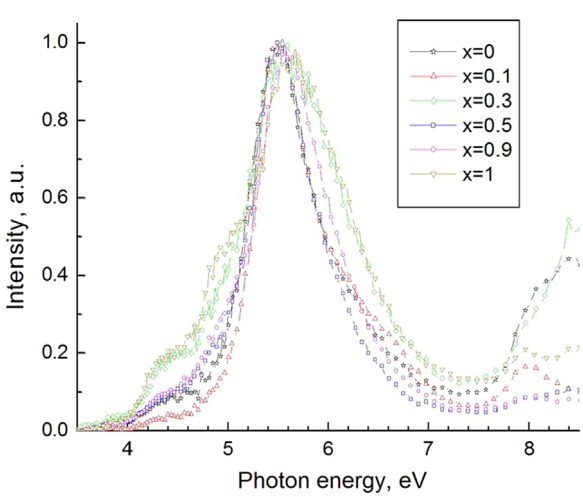

Fig. 10. The excitation spectra of $Lu_xY_{1-x}PO_4$:Eu^{3+}, $x=0$ (1); 0.1 (2); 0.3 (3); 0.5 (4); 0.9 (5); 1 (6), $\lambda_{em}=615$ nm, $T=300$ K.

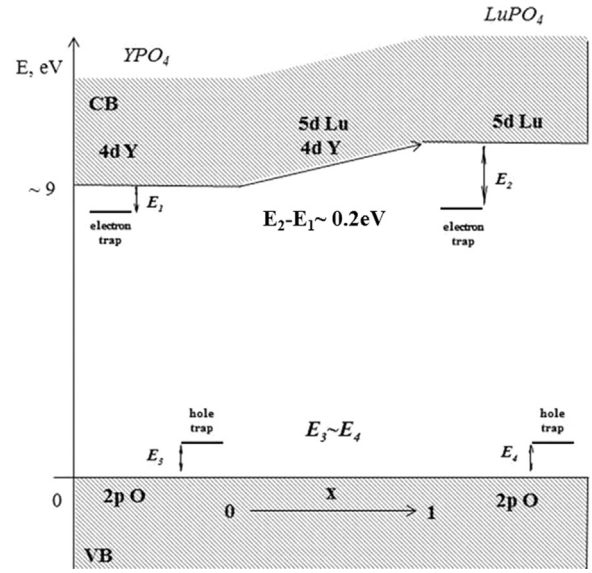

Fig. 11. Scheme of the band structure of $Lu_xY_{1-x}PO_4$ which describes the band shift with x value.

electron transitions from 2p O^{2-}, which mainly forms the VB to 4f Eu^{3+} levels located in the forbidden band. The position of CTB should not change if the top of VB is not shifted. According to Fig. 10 the CTB is a broad band in the region from 4 to 7 eV with a maximum at 5.5–5.6 eV. The band is slightly broader for the cases of $x=0.3$ and 1, however its maximum does not depend on x. Therefore this result further confirms our conclusion.

To summarize, the band gap increases with increase of the x value and it occurs as a result of modification of the CB bottom, whereas the position of the VB's top is unchanged. The scheme of the modification of energy bands and of trap state in the forbidden gap of $Lu_xY_{1-x}PO_4$ is presented in Fig. 11. The scheme is plotted in simplifying supposition that the top of VB and bottom of CB are flat.

It is worth noting that the behavior of the low-temperature TSL peaks (A and A′) of $Lu_xY_{1-x}PO_4$:Ce^{3+} differs from that of the main high-temperature peaks (B and C). The position of these peaks does not depend on the x value. This behavior cannot be explained in the terms of the simple TSL model, in which thermal release of electrons from the traps is due to a transition to CB with a subsequent radiative recombination with holes localized at Ce ions. Similar behavior has been observed previously for another set of oxide mixed crystals $Lu_xY_{1-x}AlO_3$:Ce^{3+} [37] where the lower part of CB is formed by the 4d and 5d states of the Y and Lu ions as well [38–40]. Therefore the shift of the CB bottom could be expected in $Lu_xY_{1-x}AlO_3$ similarly to $Lu_xY_{1-x}PO_4$. However the absence of the shift of TSL peaks has been observed in case of $Lu_xY_{1-x}AlO_3$:Ce^{3+} while the TSL peaks were ascribed to the release of electrons governed by a thermally assisted tunneling process from the trap to the Ce emitting center. We propose the similar mechanism to be valid for the case of TSL peaks A and A′ of $Lu_xY_{1-x}PO_4$:Ce^{3+}. In this case electrons are not released to CB, but reach the tunneling levels of the trap by thermal activation and, therefore these TSL peaks do not provide with the data on the modification of CB.

4. Conclusions

In this work we have studied the influence of the Lu/Y cations substitution in the $Lu_xY_{1-x}PO_4$:RE^{3+} (RE=Ce, Eu) mixed crystals on their structural, electronic and optical properties. The experimental studies of the TSL were supported by the ab initio

calculations of the above-mentioned properties in the whole range of the concentration *x*. The analysis of the TSL curves shows the presence of point defects in both studied sets of the phosphates. The origin of the existing defects was discussed. It was concluded that in the case of the $Lu_xY_{1-x}PO_4:Ce^{3+}$ the TSL peaks with maxima in the 90–110 K range are associated with the cerium ions, while the peaks with maxima in the 180–230 K range are connected with the host defects. The gradual shift of the position of the TSL peaks with maxima in the 180–230 K range to high-temperature with the increase of *x* value indicates the high-energy shift of the bottom of CB. In case of $Lu_xY_{1-x}PO_4:Eu^{3+}$ the TSL peaks in the 300–450 K range can be ascribed to the host defects of phosphates. The absence of considerable shift of these TSL peaks points out that the position of the top of VB does not depend on the relative concentration of Lu and Y. Therefore, the band gap gradually increases from YPO_4 to the $LuPO_4$ due to the change of the position of bottom of CB only.

The calculations of the energy bands structure confirms the experimental results and demonstrates a similar trend in the modified band gaps. According to the calculations, the top of the VB is formed mainly by the 2p states of O with a minor contribution of the 3p and 3s states of P in its lower part. The bottom of the conduction band is formed with the 4d and 5d states of substituted cations (Y and Lu), whose gradual substitution is responsible for the bandgap shift.

Acknowledgments

This work was supported by Marie Curie Initial Training Network LUMINET (Grant agreement no. 316906) and institutional research funding IUT (IUT02-26) of the Estonian Ministry of Education and Research. The financial support from Mobilitas ESF Program (Grant MTT83) is also gratefully acknowledged. Dr. G. A. Kumar (University of Texas in San Antonio) is thanked for allowing to use Materials Studio package. Financial support of Russian Ministry of Education and Science Agreement RFMEFI61614X0006 and Russian Foundation for Basic Research RFBR 15-02-07825-a are gratefully acknowledged. M.G. Brik appreciates support from the Programme for the Foreign Experts offered by Chongqing University of Posts and Telecommunications, European Regional Development Fund (Center of Excellence 'Mesosystems: Theory and Applications', TK114), and the Ministry of Education and Research of Estonia, Project PUT430, the Recruitment Program of High-end Foreign Experts (grant No. GDW20145200225) and Visiting Professorship at the Institute of Physics, Polish Academy of Sciences. We are grateful to Ivo Romet for his kind help in the analysis of experimental data.

References

[1] W.W. Moses, M.J. Weber, S.E. Derenzo, D. Perry, P. Berndahl, L.A. Boatner, IEEE Trans. Nucl. Sci. 45 (1998) 462.
[2] W.W. Moses, M.J. Weber, S.E. Derenzo, D. Perry, P. Berdahl, L. Schwarz, U. Sasum, L.A. Boatner, Recent results in a search for inorganic scintillators for X- and gamma-ray detection, in: Proceedings of the International Conference on Inorganic Scintillators and Their Applications, Chinese Academy of Sciences Press, Shanghai, China, 1997, pp. 358–361.
[3] W. Dajun, S. Xia, M. Yin, J. Rare Earths 26 (2008) 439.
[4] E. Nakazawa, J. Lumin. 100 (2002) 89.
[5] T. Justel, P. Huppertz, W. Mayr, D.U. Wiechert, J. Lumin. 106 (2004) 225.
[6] L.A. Boatner, Rev. Mineral. Geochem. 48 (2002) 87.
[7] F.X. Zhang, M. Lang, R.C. Ewing, J. Lian, Z.W. Wang, J. Hu, L.A. Boatner, J. Solid State Chem. 181 (2008) 2633.
[8] L.A. Boatner, G.W. Beall, M.M. Abraham, C.B. Finch, P.G. Huray, M. Rappaz, Monazite and Other Lanthanide Orthophosphates as Alternate Actinide Waste Forms, Scientific Basis for Nuclear Waste Management, Plenum Publishing Corporation, New York (1980), p. 289.
[9] H. Meyssamy, K. Riwotzki, A. Kornowski, S. Naused, M. Haase, Adv. Mater., 11, (1999) 840.
[10] D. Wisniewski, S. Tavernier, A.J. Wojtowicz, M. Wisniewska, P. Bruyndonckx, P. Dorenbos, E. van Loef, C.W.E. van Eijk, L.A. Boatner, Nucl. Instrum. Methods Phys. Res. Sect. A – Accel. Spectrom. Detect. Assoc. Equip. 486 (2002) 239.
[11] V.N. Makhov, N.Yu Kirikova, M. Kirm, J.C. Krupa, P. Liblik, A. Lushchik, Ch Lushchik, E. Negodin, G. Zimmerer, Nucl. Instrum. Methods Phys. Res. Sect. A – Accel. Spectrom. Detect. Assoc. Equip. 486 (2002) 437.
[12] S. Heer, O. Lehmann, M. Haase, H.-U. Gudel, Angew. Chem. Int. Ed. 42 (2003) 3179.
[13] M. Ferhi, K. Horchani-Naifer, S. Hraiech, M. Ferid, Y. Guyot, G. Boulon, Radiat. Meas. 46 (2011) 1033.
[14] S.M. Goedeke, W.A. Hollerman, S.W. Allison, P.A. Gray, L.A. Lewis, R. W. Smithwick III, L.A. Boatner, D.C. Glasgow, I.N. Ivanov, H. Wise, IEEE Trans. Nucl. Sci. 53 (2006) 2398.
[15] A.N. Belsky, C. Dujardin, C. Pedrini, A. Petrosyan, W. Blanc, J. . Gacon, E. Auffray, P. Lecoq, in: Proceedings of the Fifth International Conference on Inorganic Scintillators and Their Applications, 1999, 363.
[16] A.N. Belsky, C. Dujardin, C. Pedrini, A. Petrosyan, W. Blanc, J.C. Gacon, E. Auffray, P. Lecoq, N. Garnier, H. Canibano, IEEE Trans. Nucl. Sci. 48 (2001) 1095.
[17] Y.T. Wu, D.Z. Ding, S.K. Pan, F. Yang, G.H. Ren, Cryst. Res. Technol. 46 (2011) 48.
[18] O. Sidletskiy, A. Belsky, A. Gektin, S. Neicheva, D. Kurtsev, V. Kononets, C. Dujardin, K. Lebbou, O. Zelenskaya, V. Tarasov, K. Belikov, B. Grinyov, Cryst. Growth Des. 12 (2012) 4411.
[19] O. Sidletskiy, V. Kononets, K. Lebbou, S. Neicheva, O. Voloshina, V. Bondar, V. Baumer, K. Belikov, A. Gektin, B. Grinyov, M. Joubert, Mater. Res. Bull. 47 (2012) 3249.
[20] V.S. Levushkina, V.V. Mikhailin, D.A. Spassky, B.I. Zadneprovski, M. S. Tret'yakova, Phys. Solid State 56 (2014) 2247.
[21] A.V. Gektin, A.N. Belsky, A.N. Vasilev, IEEE Trans. Nucl. Sci. 61 (2014) 262.
[22] M. Fasoli, A. Vedda, M. Nikl, C. Jiang, B.P. Uberuaga, D.A. Andersson, K. J. McClellan, C.R. Stanek, Phys. Rev. B 84 (2011) 081102 4p.
[23] A. Lecointre, A. Bessiere, A.J.J. Bos, P. Dorenbos, B. Viana, S. Jacquart, J. Phys. Chem. C 115 (2011) 4217.
[24] A.J.J. Bos, P. Dorenbos, A. Aurelie, B. Viana, Radiat. Meas. 43 (2008) 222.
[25] F. Moretti, G. Patton, A. Belsky, M. Fasoli, A. Vedda, M. Trevisani, M. Bettinelli, C. Dujardin, J. Phys. Chem. C 118 (2014) 9670.
[26] A. Dobrowolska, A.J.J. Bos, P. Dorenbos, J. Phys. D: Appl. Phys. 47 (2014) 335301.
[27] Anne-Laure Bulin, Andrey Vasil'ev, Andrei Belsky, David Amans, Gilles Ledoux, Christophe Dujardin, Nanoscale 7 (2015) 5744.
[28] S.J. Clark, M.D. Segall, C.J. Pickard, P.J. Hasnip, M.J. Probert, K. Refson, M. C. Payne, Z. Kristallogr. 220 (2005) 567.
[29] J.P. Perdew, K. Burke, M. Ernzerhof, Phys. Rev. Lett. 77 (1996) 3865.
[30] W.O. Milligan, D.F. Mullica, G.W. Beall, L.A. Boatner, Inorg. Chim. Acta 60 (1982) 39.
[31] V.V. Mikhailin, D.A. Spassky, V.N. Kolobanov, A.A. Meotishvili, D.G. Permenov, B.I. Zadneprovski, Radiat. Meas. 45 (2010) 307.
[32] V.N. Makhov, N.Yu Kirikova,M Kirm, J.C. Krupa, P. Liblik, A. Lushchik, Ch. Lushchik, E. Negodin, G. Zimmerer. in: Proceedings of the 6th International Conference on Inorganic Scintillators and their Use in Scientific and Industrial Applications, 486, 2002, 437–442.
[33] T. Shalapska, P. Dorenbos, A. Gectin, G. Stryganyuk, A. Voloshinovskii, J. Lumin. 155 (2014) 95.
[34] J.P. Perdew, M. Levy, Phys. Rev. Lett. 51 (1983) 1884.
[35] A.H. Krumpel, A.J.J. Bos, A. Bessiere, E. Van der Kolk, P. Dorenbos, Phys. Rev. B 80 (2009) 085103.
[36] S. Erdei, L. Kovksb, M. Martini, F. Meinardi, F.W. Ainger, W.B. White, J. Lumin. 68 (1996) 27.
[37] A. Vedda, M. Martini, F. Meinardi, J. Chval, M. Dusek, J.A. Mares, E. Mihokova, M. Nikl, Phys. Rev. B 61 (2000) 8081.
[38] C. Dujardin, C. Pedrini, J.C. Gacon, A.G. Petrosyan, A.N. Belsky, A.N. Vasil'ev, J. Phys.: Condens. Matter 9 (1997) 5229.
[39] W.Y. Ching, Yong-Nian Xu, Phys. Rev. B 59 (1999) 12815.
[40] D.J. Singh, Phys. Rev. B 76 (2007) 214115.